ChemComm

COMMUNICATION

View Article Online
View Journal | View Issue

Cite this: *Chem. Commun.*, 2015, 51, 12201

Received 19th May 2015,
Accepted 25th June 2015

DOI: 10.1039/c5cc04145g

www.rsc.org/chemcomm

Stabilization of cubic Sr_2FeMoO_6 through topochemical reduction†

Daniel D. Taylor,[a] Nathaniel J. Schreiber,[a] Craig M. Brown,[bc] Angel M. Arevalo-Lopez[d] and Efrain E. Rodriguez*[ae]

Sr_2FeMoO_6 has been extensively studied for application in spintronic devices. Through the topochemical de-intercalation of oxygen anions with metal hydride reduction, we demonstrate that the high temperature cubic phase is stabilized, at room temperature, whilst leaving the magnetic ordering intact. Synchrotron X-ray and neutron powder diffraction were used to characterize the structure and stoichiometry of the reduced oxide.

Sr_2FeMoO_6 (SFMO) is a half-metal (100% spin polarization of conduction electrons) with magnetic ordering above room temperature, making it a candidate for spintronic devices.[1] This half-metallic property is closely related to the antiferromagnetic ordering of nearest neighbor B-site cations in the double perovskite structure.[2,3] Electron doping has been identified as a promising method to increase the magnetic ordering temperature in double perovskites such as SFMO.[4] However, traditional cation solid-solution techniques tend to induce lattice strain. This strain has been linked to B-site disorder, or anti-site disorder (ASD), and is therefore detrimental to long range magnetic ordering.[5,6]

In this communication, we investigate the use of anion manipulation to electron dope SFMO and show that through oxygen de-intercalation, the high temperature cubic structure can be stabilized at room temperature without loss of the magnetic ordering. Recent developments in topochemical reductions have highlighted their ability to selectively de-intercalate or substitute certain anions whilst leaving the rest of the lattice intact.[7,8] For example, $SrFeO_{3-\delta}$ has been reduced to form the metastable antiferromagnet $SrFeO_2$,[9] $SrCrO_3$ has been reduced to form the nanostructured material $SrCrO_{3-\delta}$,[10] and $LaSrCoO_4$ has been reduced to form the oxyhydride $LaSrCoO_3H_{0.7}$.[11] These reductions are performed by reacting a transition metal oxide with a strong solid-state reducing agent (*e.g.* CaH_2, NaH, LiH) at low temperatures.[12] The topochemical reduction of ordered double perovskite systems is a relatively under explored area with the only published reports focused on the $Sr_{n+1}(Fe_{0.5}Ru_{0.5})_nO_{3n+1}$ system.[13,14]

For this study, SFMO was first synthesized through the solid-state reaction of $SrCO_3$, MoO_3, and Fe_2O_3. Stoichiometric amounts of the starting materials were thoroughly ground as an acetone slurry. After a 3 hour calcination at 900 °C, pellets of the reaction mixture were heated in a tube furnace for 2.5 hours at 1200 °C under flowing 5% H_2/N_2 followed by furnace cooling. This final step was repeated three times, with intermittent grinding, to increase the crystallinity of the sample.

To prepare the reduced SFMO (SFMO-red), the oxide was ground thoroughly in a 1 : 3 mole ratio with CaH_2 in a N_2 filled glove box. Pellets of the reaction mixture were then sealed in glass ampoules (pressure $< 10^{-2}$ Torr) and heated in a box furnace at 500 °C for 3 days followed by furnace cooling. The reacted mixture was then washed with 0.15 M (mol L^{-1}) NH_4Cl/dried methanol to remove reaction byproducts. The tetragonal to cubic phase transition was observed in samples reduced at temperatures as low as 400 °C. However, in order to maximize the effects of the reaction, the highest reaction temperature that did not lead to sample decomposition (500 °C) was used for all subsequent characterization experiments.

We investigated the structures of both SFMO and SFMO-red with high resolution synchrotron powder X-ray diffraction (S-XRD) and neutron powder diffraction (NPD) experiments. S-XRD patterns were collected on beam line 11-BM at the Advanced Photon Source (APS), Argonne National Laboratory, using an average wavelength of 0.413670 Å. Constant wavelength NPD data were collected on the BT-1 diffractometer at the NCNR using a Cu(311) monochromator with a 90° take-off angle, $\lambda = 1.5398$ Å, and in-pile collimation of 60 minutes of arc. The sample was sealed in a vanadium container of length 50 mm and diameter 10.8 mm

[a] *Department of Materials Science and Engineering, University of Maryland, College Park, Maryland, 20742-2115, USA*
[b] *NIST Center for Neutron Research, National Institute of Standards and Technology, Gaithersburg, Maryland 20899, USA*
[c] *Department of Chemical and Biomolecular Engineering, University of Delaware, Newark, Delaware 19716, USA*
[d] *Centre for Science at Extreme Conditions, The University of Edinburgh, Edinburgh, EH9 3FD, UK*
[e] *Department of Chemistry & Biochemistry, University of Maryland, College Park, Maryland, 20742-4454, USA. E-mail: efrain@umd.edu*

† Electronic supplementary information (ESI) available. See DOI: 10.1039/c5cc04145g

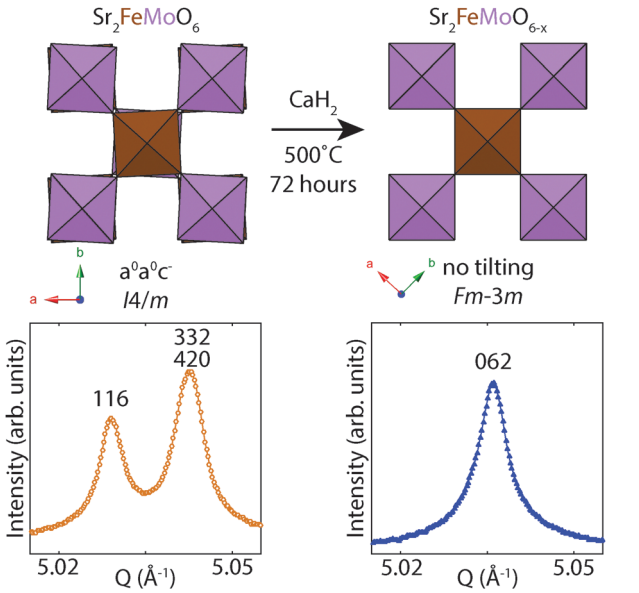

Fig. 1 Comparison of synchrotron XRD data of precursor (SFMO) and reduced (SFMO-red) materials. The reduction reaction eliminates the $a^0a^0c^-$ octahedral tilting present in the starting material. A select region of the corresponding synchrotron XRD patterns is shown as the material transitions from tetragonal (*I*4/*m*; left) to cubic (*Fm*$\bar{3}$*m*; right). The Miller indices of the depicted peaks are included for reference. Complete diffraction patterns are provided in the ESI.†

inside a dry He-filled glovebox. A furnace was used for temperature control. Rietveld refinement of S-XRD and NPD data was performed with the TOPAS 4.2[15] and FULLPROF[16] software suites.

A comparison of S-XRD data collected for SFMO and SFMO-red is presented in the bottom portion of Fig. 1. A clear phase transition can be seen as the peak splitting observed for SFMO is no longer present in SFMO-red. This phase transition is associated with the loss of $a^0a^0c^-$ (Glazer notation[17]) octahedral tilting, as is depicted in Fig. 1. Rietveld refinements were performed to quantify the affects of the reduction reaction with select parameters presented in Table 1. Complete structural parameters (Table S1, ESI†) and plots of the refinements (Fig. S1 and S2, ESI†) are given in the ESI.† The room temperature data (300 K) clearly indicate that whilst the *I*4/*m* structure fits the SFMO pattern, the *Fm*$\bar{3}$*m* structure best describes the symmetry of SFMO-red. This finding implies that the high temperature cubic structure of SFMO ($T_s \approx 420$ K)[18,19] has been stabilized at room temperature through the topochemical hydride reduction. The slight increase in ASD observed in the refinement of SFMO-red may be an indication of increased lattice disorder that stabilizes the high temperature structure down to lower temperatures.

Such a stabilization of SFMO through electron doping has been previously reported in cases of A-site substitution of rare earth metals for Sr.[20,21] However, these reports also found that lattice strain, associated with cation doping, increases the ASD on the B-site sublattice. This increase in ASD leads to a rapid degradation of the magnetic ordering and therefore also the magnetoresistive properties. Topochemical reactions offer a promising alternative to more traditional doping techniques

Table 1 Select refinement parameters for diffraction patterns collected on Sr_2FeMoO_6 and Sr_2FeMoO_{6-x} samples. ASD is the percent disorder in the B-site sublattice and rot. angle is the octahedral tilt angle. Complete refinement parameters are given in the ESI (Table S1)

	Sr_2FeMoO_6		Sr_2FeMoO_{6-x}	
Temperature	300 K	500 K	300 K	500 K
Technique	S-XRD	NPD	S-XRD	NPD
Space group	*I*4/*m*	*Fm*$\bar{3}$*m*	*Fm*$\bar{3}$*m*	*Fm*$\bar{3}$*m*
a (Å)	5.572022(7)	7.90784(6)	7.890986(7)	7.90795(6)
c (Å)	7.90426(1)	—	—	—
vol. (Å^3)	245.4069(7)	247.254(6)[a]	245.6766(6)[a]	247.264(6)[a]
ASD%	10.5(2)	—	14.0(2)	—
Rot. angle (°)	7.93	0	0	0
Bond lengths				
Fe–O1 (Å)	2.009(3)	2.003(3)	2.006(1)	2.001(4)
Fe–O2 (Å)	2.011(2)	—	—	—
Bond lengths				
Mo–O1 (Å)	1.941(3)	1.951(3)	1.939(1)	1.953(4)
Mo–O2 (Å)	1.941(2)	—	—	—
O occ.	6.03(2)	6.00(3)	5.58(2)	5.39(3)
χ^2	1.69	1.13	1.50	1.14
R_{wp}	10.09	7.33	8.38	4.72

[a] Reduced unit cell volume for comparison to *I*4/*m* structure.

because the low temperatures of the reactions should disfavor significant rearrangement of the cation sublattice.[7,8]

Due to the limited sensitivity of X-rays to oxygen and hydrogen, NPD patterns were collected for SFMO and SFMO-red at 500 K. Above the magnetic ordering temperature ($T_c \approx$ 420 K), the nuclear Bragg reflections have no contribution from the magnetic structure factor, which allows us to accurately refine the oxygen structural parameters. Fig. 2 shows the refinement of SFMO-red, and select parameters are provided in Table 1. Complete refinement parameters (Table S1, ESI†) and a plot of the SFMO refinement (Fig. S3, ESI†) are given in the ESI.† The patterns for both samples were fit using the *Fm*$\bar{3}$*m* structure and the ASD was set to the value refined from S-XRD at 300 K. Previous reports have highlighted the insensitivity of NPD to ASD with refinement results of this parameter being unreliable.[22] However, even when the ASD parameters were allowed to vary freely, the refinements revealed no significant change in oxygen parameters. Fig. S4 (given in the ESI†) depicts a comparison of the NPD patterns for both samples, where it is clear that the reduced sample has a larger background than that of the precursor oxide. A possible reason for the observed heightened background in SFMO-red is the presence of hydrogen, which has a large incoherent neutron scattering cross section.

The fits to the NPD data showed a change in the oxygen content from $Sr_2FeMoO_{6.00(3)}$ to $Sr_2FeMoO_{5.39(3)}$ for SFMO and SFMO-red, respectively. Previous efforts to reduce SFMO through more traditional methods have reported that the structure is not stable below an oxygen occupancy of $Sr_2FeMoO_{5.915}$[23] suggesting SFMO-red is a metastable phase. The determination of $Sr_2FeMoO_{5.915}$ and other oxygen stoichiometries by Kircheisen and Töpfer,[23] however, were performed at high temperatures and is therefore unlike that of $Sr_2FeMoO_{5.39(3)}$,

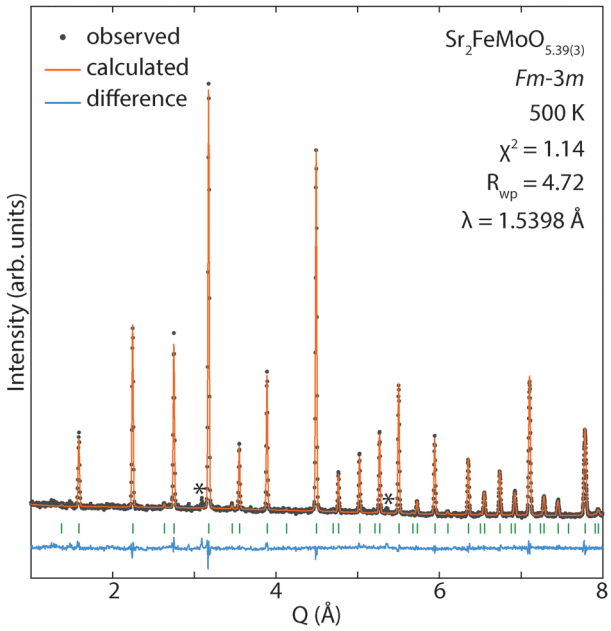

Fig. 2 Neutron powder diffraction data of the reduced material (SFMO-red) collected at 500 K. The locations of the allowed reflections are given as green tick marks below the observed and calculated patterns. The asterisks indicate the locations of peaks due to the Nb furnace.

which was prepared at low temperatures and is stable at room temperature. Interestingly, the refined parameters of the fit for SFMO-red are largely unchanged at 500 K, except for the case of the oxygen occupancy. The unit cell volume increased by only 0.004% and the B–O bond lengths are all within error of one another for both the precursor and reduced material.

Given that hydride reductions of perovskites and perovskite related phases have led to oxyhydrides such as $LaSrCoO_3H_{0.7}$[11] and $BaTiO_{3-x}H_x$,[24,25] we also considered the case where no vacancies are formed but rather H^- substitutes for O^{2-}. From this fit to the NPD data, a chemical stoichiometry of $Sr_2FeMoO_{5.63(2)}H_{0.37(2)}$ was obtained for SFMO-red. From diffraction data alone, however, we are unable to differentiate between the two scenarios – oxygen de-intercalation or hydride substitution. The Rietveld technique is only able to refine the total scattering factor of a crystallographic site, which is given by the sum of all atoms occupying the site. Both scenarios would also lead to electron doping and therefore reduction of the metal oxidation states. Although we performed thermogravimetric analysis (TGA) measurements of SFMO-red under a stream of pure O_2 for chemical analysis, the TGA results did not further elucidate whether SFMO-red is an oxyhydride, a reduced oxide, or an oxide with hydroxyl groups since SFMO-red disproportionated to Mo-deficient SFMO and $SrMoO_4$. This result is unsurprising given that SFMO is formed under reducing conditions (5% H_2/N_2) and SFMO-red itself is metastable.

To further explore the possible presence of H in this material, we performed prompt gamma activation analysis (PGAA) on both SFMO and SFMO-red at the NG-7 beam line at the NCNR. This spectroscopic technique allows for the accurate compositional analysis of elements in bulk samples. The analysis provided two interesting results. First, there is a measurable amount of H in the starting material, SFMO (H : Mo = 0.093(4)). Second, the H content increases significantly with the reduction reaction with H : Mo = 0.246(8) for SFMO-red. The surprising presence of hydrogen in the precursor material likely arises from the preparation of SFMO under the 5% H_2/N_2 stream and points to possible H content missed in previous studies of SFMO. Inelastic neutron scattering investigations are underway to elucidate the nature of H as being either protic (H^+) or hydritic (H^-) in these materials as PGAA does not probe this property. To remove surface water prior to analysis, both samples were dried overnight at 150 °C under vacuum.

Magnetic properties were measured using a magnetic property measurement system (Quantum Design MPMS XL) in DC mode. Fig. 3 presents a comparison of the hysteresis loops obtained for both SFMO and SFMO-red at 2 K. The saturated magnetic moment (M_s), obtained under an applied magnetic field of 5 Tesla, was 3.44 μ_B and 3.14 μ_B for SFMO and SFMO-red, respectively. The M_s of SFMO agrees well with values found in the literature for samples containing approximately 10% ASD.[26] The decrease in M_s is expected with the reduction as the conduction band, which is aligned anti-parallel to the ferromagnetic moment, is populated by electrons.

A schematic representation of the spin-polarized density of states (DOS) is presented as an inset to Fig. 3. As the Fermi level increases (given as the dashed vertical line) into the spin down polarized conduction band, it can be seen that the net magnetic

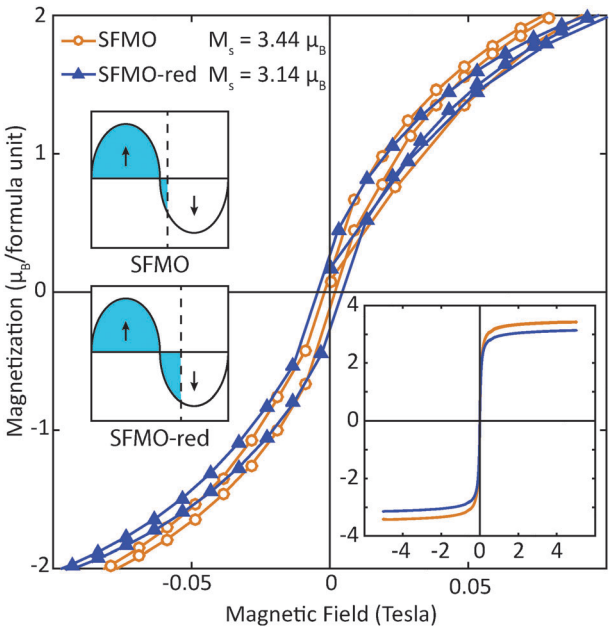

Fig. 3 Magnetic hysteresis loops of the starting material Sr_2FeMoO_6 (SFMO) and the reduced product $Sr_2FeMoO_{5.39(3)}$ (SFMO-red). The reduced material displayed a decrease in the saturated magnetic moment (M_s = 3.14 μ_B), compared to the starting material (M_s = 3.44 μ_B), as expected with electron doping. The reduced material also showed a slight increase in the coercive field. The inset density of states schematics illustrate how the filling of the conduction band (spin down) would affect the M_s value. The Fermi level is indicated by the dashed vertical line.

moment will decrease as the up and down spin polarized electrons cancel out. Population of the spin-down band, which is primarily of Fe and Mo t_{2g}-character,[2] could explain the stabilization of the cubic structure in SFMO-red. Such electronic stabilization is well known in metallic perovskite oxides such as ReO_3 and Na_xWO_3, where filling of a metal t_{2g} band causes linear O–M–O bond angles and low electrical resistivity.[27]

To assess the effect of the reduction reaction on T_c, the magnetization was determined as a function of temperature (Fig. S5 in the ESI†). Whilst it is difficult to determine the exact temperature of the phase transition, it is apparent that T_c has not been largely affected and the magnetic ordering remains above 400 K. This finding implies that structural and magnetic phase transitions no longer coincide. Previous reports have established that these phase transitions are not coupled and doping can be used to affect them differently.[5] In these cases, however, the magnetic ordering was only ever observed in the tetragonal phase with the exception being cubic $Sr_{2-x}Eu_xFeMoO_6$.[28] Here, we have demonstrated that through the topochemical de-intercalation of oxygen atoms, we can stabilize the cubic phase at room temperature whilst leaving the magnetic ordering intact.

Fig. S6, provided in the ESI,† depicts a plot of *M vs. H* data taken for SFMO and SFMO-red at 500 K. Here we can see that both SFMO and SFMO-red behave paramagnetically, as expected for a material above its T_c. However, the curve for SFMO-red, does not cross through the origin. This suggests there may be a small ferromagnetic impurity not detectable in any of our diffraction experiments.

In conclusion, we synthesized a reduced form of Sr_2FeMoO_6 through a topochemical reduction reaction with CaH_2. Unlike its precursor, the new reduced oxide is cubic at room temperature whilst its magnetic ordering, known to be responsible for its magnetoresistive properties, remains intact. This is the first time that cubic SFMO has been stabilized at room temperature with such a large oxygen substoichiometry, demonstrating the promise of hydride reduction as a tool for the preparation of metastable functional materials. Our study highlights the possibility of using anion manipulation as a means to modulate the structure of functional materials as an alternative to traditional techniques of cation doping. A high incoherent background observed in the neutron diffraction data of SFMO-red and PGAA measurements indicate that the H content of the material may be responsible for the stabilization of SFMO-red. Ongoing studies on the hydride reduction of $Sr_2Fe_{1+x}Mo_{1-x}O_6$ solid solutions will further establish the role of the B cation in perovskites for either the de-intercalation of oxide anions or substitution of oxide by hydride.

Use of the Advanced Photon Source at Argonne National Laboratory was supported by the U.S. Department of Energy, Office of Science, Office of Basic Energy Sciences, under Contract No. DE-AC02-06CH11357. We also acknowledge the support of the National Institute of Standards and Technology, U.S. Department of Commerce, in providing the neutron research facilities used in this work. Certain commercial equipment, instruments, or materials are identified in this document. Such identification does not imply recommendation or endorsement by the National Institute of Standards and Technology nor does it imply that the products identified are necessarily the best available for the purpose. We thank the University of Maryland for its funding support.

References

1 K. L. Kobayashi, T. Kimura, H. Sawada, K. Terakura and Y. Tokura, *Nature*, 1998, **395**, 677–680.
2 D. Sarma, P. Mahadevan, T. Saha-Dasgupta, S. Ray and A. Kumar, *Phys. Rev. Lett.*, 2000, **85**, 2549–2552.
3 C. J. Howard, B. J. Kennedy and P. M. Woodward, *Acta Crystallogr., Sect. B: Struct. Sci.*, 2003, **59**, 463–471.
4 M. Tovar, M. T. Causa, A. Butera, J. Navarro, B. Martinez, J. Fontcuberta and M. C. G. Passeggi, *Phys. Rev. B: Condens. Matter Mater. Phys.*, 2002, **66**, 1–5.
5 D. Serrate, J. M. D. Teresa and M. R. Ibarra, *J. Phys.: Condens. Matter*, 2007, **19**, 023201.
6 O. Erten, O. N. Meetei, A. Mukherjee, M. Randeria, N. Trivedi and P. M. Woodward, *Phys. Rev. Lett.*, 2011, **107**, 257201.
7 T. Yamamoto and H. Kageyama, *Chem. Lett.*, 2013, **42**, 946–953.
8 M. A. Hayward, *Semicond. Sci. Technol.*, 2014, **29**, 064010.
9 Y. Tsujimoto, C. Tassel, N. Hayashi, T. Watanabe, H. Kageyama, K. Yoshimura, M. Takano, M. Ceretti, C. Ritter and W. Paulus, *Nature*, 2007, **450**, 1062–1065.
10 A. M. Arévalo-López, J. A. Rodgers, M. S. Senn, F. Sher, J. Farnham, W. Gibbs and J. P. Attfield, *Angew. Chem., Int. Ed. Engl.*, 2012, **51**, 10791–10794.
11 M. A. Hayward, E. J. Cussen, J. B. Claridge, M. Bieringer, M. J. Rosseinsky, C. Kiely, S. J. Blundell, I. M. Marshall and F. L. Pratt, *Science*, 2002, **295**, 1882–1884.
12 M. A. Hayward, M. A. Green, M. J. Rosseinsky and J. Sloan, *J. Am. Chem. Soc.*, 1999, **121**, 8843–8854.j
13 F. Denis Romero, S. J. Burr, J. E. McGrady, D. Gianolio, G. Cibin and M. A. Hayward, *J. Am. Chem. Soc.*, 2013, **135**, 1838–1844.
14 F. Denis Romero, D. Gianolio, G. Cibin, P. A. Bingham, J.-C. D'Hollander, S. D. Forder and M. A. Hayward, *Inorg. Chem.*, 2013, **3**, 10920–10928.
15 R. W. Cheary and A. Coelho, *J. Appl. Crystallogr.*, 1992, **25**, 109–121.
16 J. Rodrguez-Carvajal, *Phys. B*, 1993, **192**, 55–69.
17 A. M. Glazer, *Acta Crystallogr., Sect. B: Struct. Sci.*, 1972, **28**, 3384–3392.
18 O. Chmaissem, R. Kruk, B. Dabrowski, D. Brown, X. Xiong, S. Kolesnik, J. Jorgensen and C. Kimball, *Phys. Rev. B: Condens. Matter Mater. Phys.*, 2000, **62**, 14197–14206.
19 S. Nakamura and K. Oikawa, *J. Phys. Soc. Jpn.*, 2003, **72**, 3123–3127.
20 D. Serrate, J. M. Teresa, J. Blasco, M. R. Ibarra, L. Morellon and C. Ritter, *Eur. Phys. J. B*, 2004, **39**, 35–40.
21 Q. Zhang, G. Rao, Y. Xiao, H. Dong, G. Liu, Y. Zhang and J. Liang, *Phys. B*, 2006, **381**, 233–238.
22 Q. Zhang, G. Liu and G. Rao, *Solid State Commun.*, 2006, **138**, 294–298.
23 R. Kircheisen and J. Töpfer, *J. Solid State Chem.*, 2012, **185**, 76–81.
24 Y. Kobayashi, O. J. Hernandez, T. Sakaguchi, T. Yajima, T. Roisnel, Y. Tsujimoto, M. Morita, Y. Noda, Y. Mogami, A. Kitada, M. Ohkura, S. Hosokawa, Z. Li, K. Hayashi, Y. Kusano, J. E. Kim, N. Tsuji, A. Fujiwara, Y. Matsushita, K. Yoshimura, K. Takegoshi, M. Inoue, M. Takano and H. Kageyama, *Nat. Mater.*, 2012, **11**, 507–511.
25 T. Yajima, A. Kitada, Y. Kobayashi, T. Sakaguchi, G. Bouilly, S. Kasahara, T. Terashima, M. Takano and H. Kageyama, *J. Am. Chem. Soc.*, 2012, **134**, 8782–8785.
26 L. Balcells, J. Navarro, M. Bibes, A. Roig, B. Martinez and J. Fontcuberta, *Appl. Phys. Lett.*, 2001, **78**, 781.
27 F. Cora, M. Stachiotti, C. Catlow and C. Rodriguez, *J. Phys. Chem.*, 1997, **5647**, 3945–3952.
28 Q. Zhang, Y. Xiao, Z. Xu, G. Liu, J. Li and G. Rao, *J. Solid State Chem.*, 2010, **183**, 2432–2437.

